의학박사 학위논문

Three-Dimensional Kinematic Comparison of Dart-Throwing Motion Between the Wrists with Malunited Distal Radius and the Contralateral Normal Wrists Using CT Images

원위 요골 부정유합과 반대편 정상 수근 관절 간의 다트 던지기 운동의 CT 영상을 이용한 삼차원 동력학적 비교

2012 년 8 월

서울대학교 대학원

의학과 정형외과학 전공

이 상 림

A thesis of the Degree of Doctor of Philosophy

원위 요골 부정유합과 반대편 정상 수근 관절 간의 다트 던지기 운동의 CT 영상을 이용한 삼차원 동력학적 비교

Three-Dimensional Kinematic Comparison of Dart-Throwing Motion Between the Wrists with Malunited Distal Radius and the Contralateral Normal Wrists Using CT Images

August 2012

The Department of Orthopedic Surgery

Seoul National University

College of Medicine

Sanglim Lee

Three-Dimensional Kinematic Comparison of Dart-Throwing Motion Between the Wrists with Malunited Distal Radius and the Contralateral Normal Wrists Using CT Images

지도 교수 백 구 현

이 논문을 의학박사 학위논문으로 제출함

2012년 4월

서울대학교 대학원

의학과 정형외과학 전공

이 상 림

이상림의 의학박사 학위논문을 인준함

2012년 7월

위 원 장 권 성 택 (인)

부위원장 백 구 현 (인)

위 원 이 영 호 (인)

위 원 홍 성 환 (인)

위 원 김 병 성 (인)

Three-Dimensional Kinematic Comparison of Dart-Throwing Motion Between the Wrists with Malunited Distal Radius and the Contralateral Normal Wrists Using CT Images

by
Sanglim Lee

April 2012

A thesis submitted to the Department of Orthopedic Surgery in partial fulfillment of the requirement of the Degree of Doctor of Philosophy in Medicine at Seoul National University College of Medicine

July 2012

Approved by Thesis Committee:

Professor Sung-Tack Kwon Chairman

Professor Goo Hyun Baek Vice chairman

Professor Young Ho Lee

Professor Sung Hwan Hong

Professor Byung Sung Kim

Abstract

Introduction: The purpose of this study was to compare motion of the capitate, scaphoid, and lunate in wrists with a malunited distal radius and contralateral normal wrists during dart-throwing motion (DTM) by three-dimensional kinematic studies using computed tomography images.

Methods: Six patients with unilateral distal radius malunion were recruited and computed tomography was performed simultaneously on both wrists at 5 stepwise positions simulating dart-throwing motion. The average rotation, translation, and lengths of moment arm of the capitate, scaphoid, and lunate were calculated and compared between both wrists by using the concept of helical axis motion. The helical motion of the capitate was also evaluated in a scaphoid- and lunate-based coordinate system. The orientation of the helical axes and the locations of centers of motion were compared between the wrists.

Results: The average rotation of the capitate around its own helical axis was larger in the uninjured wrist, but the average translation and lengths of the moment arms were not statistically different. The average rotation, translation, and lengths of the moment arms of the scaphoid and lunate were not significantly different between the wrists. The capitate rotated more in the scaphoid- or lunate-based coordinate system in the uninjured wrist. The orientations of the helical axes of the capitate, scaphoid, and lunate were not significantly different. The centers of helical axis motion of the 3 carpal bones were located more dorsally and radially in the injured wrist. As the radial inclination of the distal radius decreased, radial displacement of the centers of helical axis motion of the 3 carpal bones tended to increase. As the dorsal tilt of the distal radius increased, dorsal displacement of the centers of helical axis

motion of the 3 carpal bones tended to increase.

Conclusions: This study showed that decreased DTM in wrists with distal radius malunion resulted from decreased midcarpal motion. As DTM is a crucial motion of the wrist joint, the result suggests that anatomical reduction of distal radius fractures should be performed to maintain the wrist function.

Keywords: Distal radius malunion, dart-throwing motion, carpal kinematics, three-dimensional, CT.

Student Number: 2007-30509

CONTENTS

LIST OF TABLES

LIST OF FIGURES

INTRODUCTIONS

There have been reports suggesting that long-term outcomes of conservative treatment for distal radius fractures are favorable. Although a radiological assessment of 106 patients with malunited distal radius fractures in the study of Forward and coworkers[1] showed that a higher grade of osteoarthritis was present on the fractured side in 43% of patients, in a long-term follow-up, 65% had mild narrowing of the joint space with grade 0 or 1 arthritis, even with intraarticular fractures. The clinical result was worse in the injured wrist and the difference was statistically significant, as assessed by the Patient Evaluation Measure, but the authors suggested that this might not be clinically significant because of the small difference (<10%) of the lowest threshold in the score. The average Disabilities of the Arm, Shoulder and Hand (DASH) score was also significantly different between the intra-articular and extra-articular injuries, and the authors proposed that the mean DASH score might not have clinical relevance because it was similar to that of a comparative "control" population in North America. The authors ultimately concluded that the long-term clinical outcome of intra-articular fractures might not be as poor and that imperfect reduction of the fractures

might not result in symptomatic arthritis. Meanwhile, another follow-up study of 87 nonsurgically treated distal radius fractures indicated that a number of patients continued to experience some hand/wrist impairment several years after the trauma, and the severity of fracture displacement seemed to influence the clinical outcome.[2]

Malunion of the distal radius can result in various complications such as persistent pain, limited range of motion of the wrist and forearm, weakness of grip, nerve irritation or entrapment, tendon ruptures, carpal instability, and arthritis of the distal radioulnar or radiocarpal joint. Many investigators believe that a dorsal angulation deformity after distal radius fractures will alter wrist mechanics and be the primary cause of disabilities.[3-6] Grip strength, performance of activities of daily living, and range of motion were significantly worse in wrists with dorsal angulation >12° than in wrists with dorsal angulation <10°.[5]

Carpal malalignment is seen in some wrists with a dorsally angulated distal radius, and is thought to be associated with functional outcomes.[3] Malalignment of the carpal bones is accepted as an inevitable response to the altered mechanics caused by a malunited distal radius, and 2 types have been

suggested.[7] Type 1 is midcarpal malalignment, in which the proximal carpal row extends in line with the dorsally angulated articular surface of the distal radius and the distal carpal row flexes in compensation.[8] This type of carpal instability produces dorsal intercalated segmental instability (DISI). This is considered an adaptive midcarpal instability of midcarpal subluxation. Type 2 is radiocarpal malalignment, in which all carpal bones translate dorsally with respect to the distal radius. Realignment is frequently accomplished through palmar flexion at the radiolunate joint relative to the dorsally oriented distal articular surface of the radius. The lunate and capitate remain collinear and shift together up the abnormal dorsal slope of the distal radius to a position that is dorsal to the forearm axis.[9,10] Fernandez[11] reported frequent dorsal subluxation when dorsal tilt was >35° and demonstrated that active wrist flexion increased dorsal subluxation with localized pain at the radiocarpal joint. Park et al[12] thought that individual characteristics of the extrinsic carpal ligaments might be the most important factor for determining types of carpal malalignment after dorsally angulated distal radius fractures. They suggested that more lax joints tended to show adaptive midcarpal instability patterns.

Carpal malalignment results in abnormal overload of the radiocarpal and midcarpal joint and can cause ligament attenuation, synovitis, and progressive dynamic instability.[8,12] A corrective osteotomy in the malunited distal radius is usually recommended to relieve symptoms in the wrist and to correct the carpal malalignment. Verhaegen et al[7] reported that distal radial osteotomy is a reliable technique for correction of the deformity at the distal radius with either radiocarpal or midcarpal malalignment. They showed that in the midcarpal malalignment, the preoperative and postoperative effective radiolunate flexion (ERLF) was considered normal, while in the radiocarpal malalignment group, there was a significant effect on the ERLF that could not be completely restored. Incomplete correction of the dorsal tilt after osteotomy was suggested as a cause for the incomplete correction.

Jupiter and Fernandez[13] described the criteria of malunion: radial angulation <20º, dorsal angulation beyond neutral, and shortening of ≥2 mm in comparison with the contralateral wrist. The degree of dorsal angulation is believed to be the important factor in determining corrective osteotomy. However, the amount of acceptable deformity and the indications for corrective osteotomy of the distal radius fractures are not in consensus.[14-17]

Fernandez[18] reported that deformities of the distal radius usually become symptomatic if the angulation of the distal articular surface of the radius is >25–30° in the sagittal or frontal plane, especially in young, active patients. Short et al[19] confirmed that joint compression and shear forces were altered after 25° dorsal angulation. Melendez[15] suggested that the indication for surgery for a radius malunion is palmar tilt of >18° or significant collapse or shortening of the radius. In most cases, patients who underwent corrective osteotomy had preoperative a range of dorsal angulation of >20°. Park et al[12] recommended that dorsal angulation >15° and the amount of midcarpal flexion of the DISI deformity should be the determining factors to perform corrective osteotomy.

In most activities of the wrist, the hand moves along a path from radial extension (combined radial deviation and extension) to ulnar flexion (combined ulnar deviation and flexion),[20] and this is commonly referred to as dart-throwing motion (DTM). Actually, DTM is one of the most essential human wrist motions.[21,22] A modified or squeeze form of a power grip enables a cylindrical object to be held obliquely in the palm, so that the axis of the tool becomes collinear with the axis of the forearm in the swing phase

of tool use. A power swing can be generated by a power squeeze grip and simultaneous wrist motion by wrist radial extension in a cocking phase and ulnar flexion in a swing phase.[23] This lengthens the tool's lever arm, accelerates the tool, and amplifies the wrist torque generated from the powerful forearm musculature. The potential impact power increases, as the wrist can move through a large range of motion while grasping the tool. During the swing phase, the shoulder, the elbow, and the wrist can contribute to accelerating the tool, maximizing its velocity just before impact.

Capener[24] described in 1956 that radial deviations of the wrist are most easily carried out with extension, and ulnar deviations with flexion. This DTM action corresponds with the action of the radial carpal extensors and the flexor carpi ulnaris, respectively. Palmer et al[20] were the first to investigate this oblique motion quantitatively in 1985 using a triaxial electrogoniometer. They found that many daily tasks were performed by moving the wrist from a radially extended position to a less extended ulnar-deviated position and they first described this type of motion as a DTM. They suggested that the orientation of this plane varied among activities and even among individuals performing the same activity. Midcarpal motion is

known to be the mainstay of DTM and is difficult to analyze by two-dimensional images.

Until the mid-1990s, most kinematic studies were performed in vitro, usually with markers inserted in the carpal, metacarpal, and forearm bones. Development of computerized analytic technologies has enabled noninvasive in vivo motion analysis,[25-28] which is more physiologic than in vitro motion analysis using cadavers. These techniques utilize image registration and can reconstruct 3D models with computed tomography (CT)[29] or magnetic resonance imaging (MRI).[22,30] Radiation exposure is unavoidable in acquisition of CT images, but CT scanning is more informative for bony structures and registration from CT images is accomplished more easily, because MR images have more diverse contrast of signals, which makes automatic segmentation more difficult and requires more manual delineation. There are 2 techniques of registration, surface-based and volume-based. Volume-based registration methods may have an advantage in that feature calculation is straightforward and the accuracy of these methods is likely to be unaffected by segmentation errors. Goto et al[22] have shown that volume-based registration is significantly more accurate than surface-based

registration.

Several 3D wrist motion studies have examined wrist flexion-extension motion[29] and radio-ulnar deviation.[27,31,32] Since the mid-2000s, carpal kinematics have been evaluated during DTM as well as during flexion/extension and radioulnar deviation,[22,33,34] and development of 3D imaging techniques and computerized analytic technologies has enabled noninvasive in vivo motion analysis of the wrist joint.[25-28]

Moritomo et al[35] observed that midcarpal motion during radioulnar deviation could be approximated as rotation in a plane of radiodorsal/ulnopalmar rotation of the wrist, which may coincide with DTM. The direction of scaphotrapeziotrapezoidal (STT) motion was observed in the DTM plane during both wrist flexion-extension and radioulnar deviation in cadavers with optoelectronic stereophotogrammetric motion analysis.[36]

Li et al[37] investigated in vivo coupling between wrist flexion-extension and radioulnar deviation with light-reflective surface markers attached to the forearm and hand. They found that the maximal motion boundary of all wrist circumduction cycles was egg-shaped, with maximum extension at a slight radial deviation position and maximum flexion at a slight ulnar deviation

position. This suggests that a DTM oblique to the sagittal plane will allow more motion than a pure flexion-extension motion, as DTM utilizes the midcarpal joint to a great extent.

Goto et al[22] and Moritomo et al[30,33,35] investigated in vivo kinematics of the midcarpal joint using a noninvasive bone registration technique. The DTM plane was found to be 31° from the sagittal plane[33] and the average contribution of the radiolunate joint to the global wrist motion was 26%.[22] During their DTM, the directions of rotation in the midcarpal and radiocarpal joints were similar and synergistic to each other, which may explain why the DTM plane is the usual plane of utilization of the wrist. They suggested that a DTM may be the most stable and controlled motion of the wrist.

Werner et al[38] used an electromagnetic measuring system and found that the scaphoid, lunate, and triquetrum moved less than the total wrist motion and showed out-of-plane motions in the wrist's DTM plane. Ishikawa et al[39] found that the percentage contributions of radiolunate rotation in radial extension (42%) and in ulnar flexion (39%) were less than those in pure extension (47%) and pure flexion (53%) with the use of a magnetic tracking

device in cadavers. Werner et al[40] measured in vitro scaphoid and lunate motion during 9 variations of wrist motion ranging from a pure flexion-extension motion to 7 DTMs, and finally to a pure radioulnar deviation motion. They demonstrated during intermediate motions of DTM that scaphoid movement was as little as 26% of the global wrist motion, and lunate movement as little as 22%. In the case of the minimal scaphoid motion, the DTM plane was aligned 45° from the sagittal plane. When the lunate moved minimally, the DTM was aligned 37° from the sagittal plane. Crisco et al[41] measured in vivo scaphoid and lunate motion throughout the entire range of wrist motion. They identified scaphoid motion approaching zero in a DTM plane approximately 45° from the sagittal plane, and there was minimal lunate motion in a plane approximately 30° from the sagittal plane. These findings suggest that specific rehabilitation protocols could be designed to limit radiocarpal motion while maintaining some wrist motion.[40,41] However, the specific DTM plane of minimal carpal motion may vary depending on the individual and on which carpal bone needs the least motion.

The present study was designed to evaluate the kinematics of the carpal

bones in wrists with distal radius malunion during DTM and to compare the motion of the capitate, scaphoid, and lunate in the affected wrist and the contralateral normal wrist during DTM by 3D kinematic studies using CT images.

MATERIALS AND METHODS

1. Subjects

Six patients, 4 men and 2 women, with an average age of 64 years (range, 49–81), who had unilateral distal radius malunion (4 of the left wrist), were recruited for this study with the approval of the Institutional Review Board of Sanggye Paik Hospital. The patient volunteers were screened for a history of wrist trauma, and bilateral posteroanterior, lateral, and billiards radiographs were obtained to exclude contralateral wrist injury and to confirm dorsal tilt >10°, radial inclination <10°, or radial shortening >5 mm in the affected wrist. Exclusion criteria were any history or findings of prior operation in the wrist, any wrist disease or carpal injury, distal ulnar fractures except of the ulnar styloid tip, any neurologic deficit, and stiffness in the hand. Patient examinations included passive range of motion. Five of the 6 patients were right handed and 1 patient with left distal radius malunion was ambidextrous. The average interval between trauma and CT scanning was 10 months (range 8–13 months).

2. Scanning

CT (Aquilion 64 CT System, Toshiba Medical Systems Corporation, Otawara, Japan; 120 kVp, 250 mA, 0.5 sec) was performed simultaneously on both wrists of all patients with an image slice thickness of 1.0 mm. Patients were placed in a prone position on the CT table with the forearm extended, and gripped a custom-designed wrist-positioning jig (Fig. 1) as they simulated DTM. Scans were acquired at 5 stepwise positions from full radial extension to full ulnar flexion: (1) maximum radial extension; (2) mid-radial extension; (3) neutral; (4) mid-ulnar flexion; and (5) maximum ulnar flexion. Scanning was performed proximally up to the mid-forearm to reconstruct the intact part of the radial shaft and to establish the orthogonal reference coordinate system, defining the Z-axis as the longitudinal axis of the radial shaft.

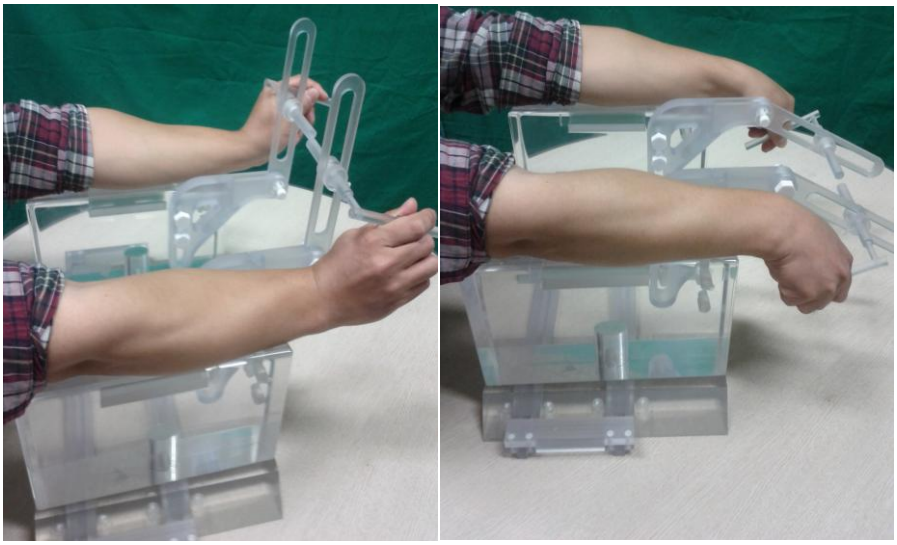

Figure 1. A custom-designed jig.

A custom-designed jig helps a patient simulating DTM.

3. Bone Segmentation and Reconstruction

Digital models of the bone were generated from the CT DICOM files. The thresholding and edge-detection algorithms in Analyze (Mayo Clinic Foundation, Rochester, MN, U.S.A.) image processing software were used (window level/width = 300/2000, thresholding value = 300). Manual intervention was occasionally necessary to define the bone contours and to eliminate contour breaks where noise and differences in bone density were prominent or the interarticular distances were small. The contours were then stacked, edited, and grouped into a voxel model using MATLAB

(MathWorks, Natick, MA, U.S.A.), which was converted into a volume model by flood-fill operation. The left wrists were converted to the right wrists to simplify the kinematic analysis.

4. Reference Coordinate System

The carpal bone motions were described in relation to an anatomically-based reference coordinate system constructed in the distal radius (Fig. 2) that was similar to that of Moritomo et al[33] However, some modifications were needed because the distal part of the radius in the injured wrists was displaced and rotated, so that the normal coordinate system could not be directly applied. The Z-axis was placed parallel to the longitudinal axis of the radial shaft, around which pronation and supination are presented (+Z was distal). The X-axis was along the bisecting line of the sigmoid notch to the radial styloid tip and perpendicular to the Z-axis (+X was radial) (Fig. 3). Rotation around the X-axis is dorsal extension and volar flexion. The origin in this coordinate system was set as the intersection of the X-axis with the interfossa ridge on the radial articular surface (Fig. 3). The Y-axis was aligned perpendicular to both the Z-axis and Y-axis and rotation around the

Y-axis represented ulnar and radial deviation (+Y was dorsal).

Figure 2. The anatomical reference coordinate system.

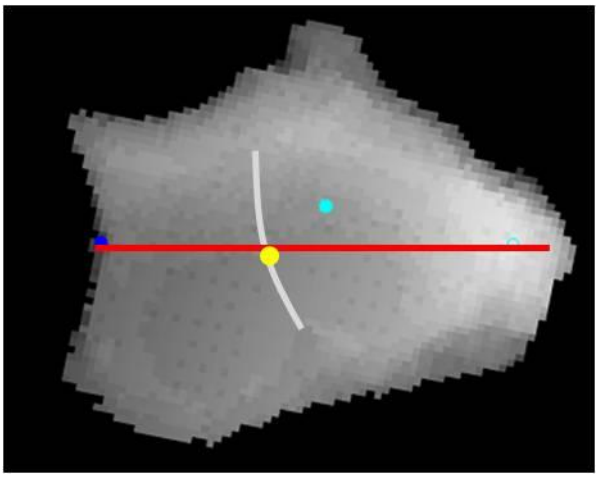

Figure 3. The reference coordinate system constructed on the articular surface of the distal radius.

Red line shows the X-axis along the bisecting line of the sigmoid notch to the radial styloid tip. The origin (yellow dot) in this coordinate system was set as the intersection of the X-axis with the interfossa ridge (white line) on the radial articular surface. Sky blue dot shows the projected point on the radial articular surface from the Z-axis.

5. Kinematic Analysis

The volume, centroid location, and orientation of the principal inertial axis for each bone were calculated from the volume models using MATLAB software. The volumes of the same carpal bone at 5 positions in the same wrist were calculated to determine the accuracy of the registration methods in this study. Accuracies were determined using the average and standard deviation of the maximum % errors of the estimated volume.

To describe the complex 3D motion of the carpal bones, helical axes of motion from position 1 (maximum radial extension) to position 5 (maximum ulnar flexion) were used (Fig. 4). The helical axis of motion uniquely describes any 3D motion as the rotation of a rigid body around, and its translation along, a single axis in space.[42] If the translation is not significant,

then the helical axis of motion can be considered a pure rotation.[29] The length of moment arm was the distance from the centroid of the carpal bone to the helical axis. We calculated the average rotation, translation, and length of the moment arms for the capitate, scaphoid, and lunate around their own helical axes. Positive translation is toward the direction of helical axis vector.

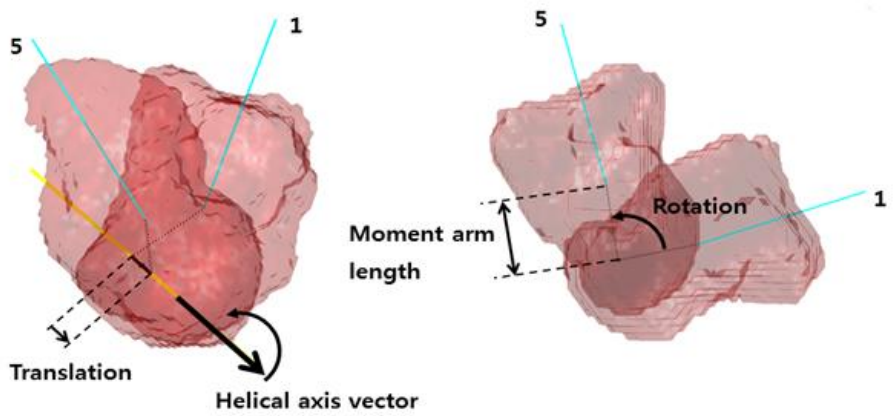

Figure 4. The helical axis motion of the capitate.

The kinematics of a capitate during dart-hrowing motion from position 1 (maximum radial extension) to 5 (maximum ulnar flexion) was described using a helical axis (Cyan solid line= the major axis of the capitate; yellow solid line= the helical axis of capitate motion; black dotted line= a line perpendicular to the helical axis from the centroid of capitate).

The helical motion of the capitate was also evaluated in the coordinate system constructed with the principal inertial axis of the scaphoid (or lunate) to compare midcarpal motion between the injured and uninjured wrists. The average rotation, translation, and length of the moment arm of the capitate in the scaphoid- or lunate-based coordinate system was calculated and compared by statistical analysis using Wilcoxon signed rank test.

The helical axis of the capitate could be regarded as the rotational axis of DTM. The orientation of the helical axis was described by the axial projection angle (θ_{XY}) between +X-axis (radial) and the projected line from the helical axis on the XY (axial) plane, the sagittal projection angle (θ_{YZ}) between +Y-axis (dorsal) and the projection line on the YZ (sagittal) plane, and the coronal projection angle (θ_{ZX}) between +Z-axis (dorsal) and the projection line on the ZX (coronal) plane (Fig. 5). The orientations of the helical axes of the capitate, scaphoid, and lunate were compared between the injured and the uninjured wrists by 3 projection angles. The orientations of the helical axes of the capitate in the scaphoid- or lunate-based coordinate systems were also compared.

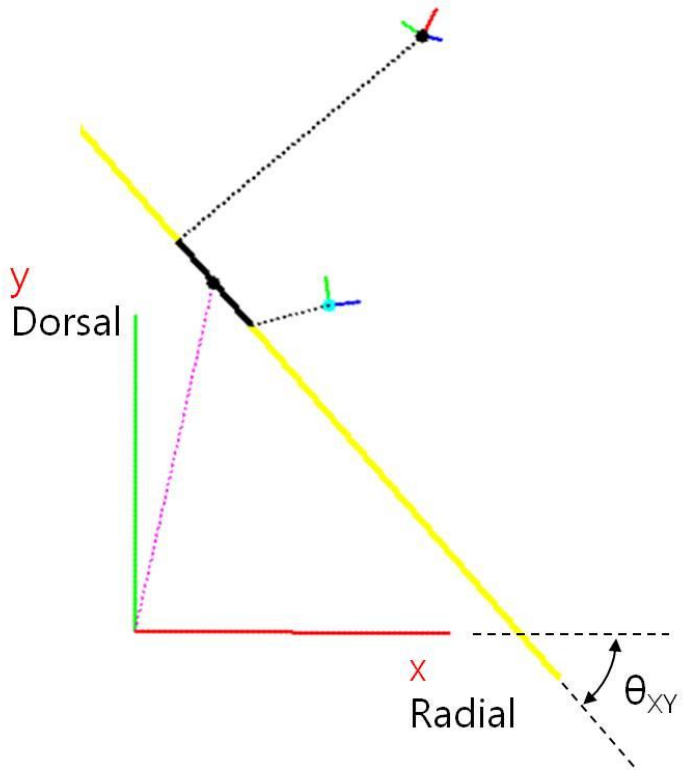

Figure 5. Axial projection angle (θ_{XY}).

Axial projection angle (θ_{XY}) was calculated by the angle between +X-axis (radial) and the projected line from the helical axis on the XY (axial) plane.

The center of the helical axis motion was defined the midpoint of translation between 2 points nearest the centroid of the carpal bone along the helical axis during rotation and translation. It was described by the distance (D) from the origin of the reference coordinate system and the angle from

the Z-axis in the coronal plane ($\varphi_{coronal}$) and the sagittal plane ($\varphi_{sagittal}$) (Fig. 6).

We assumed that the location of the center of helical axis motion for the carpal bone was related to the severity of the distal radius malunion. The correlation between radial inclination and $\varphi_{coronal}$ and between dorsal tilt and $\varphi_{sagittal}$ was investigated and compared in both wrists.

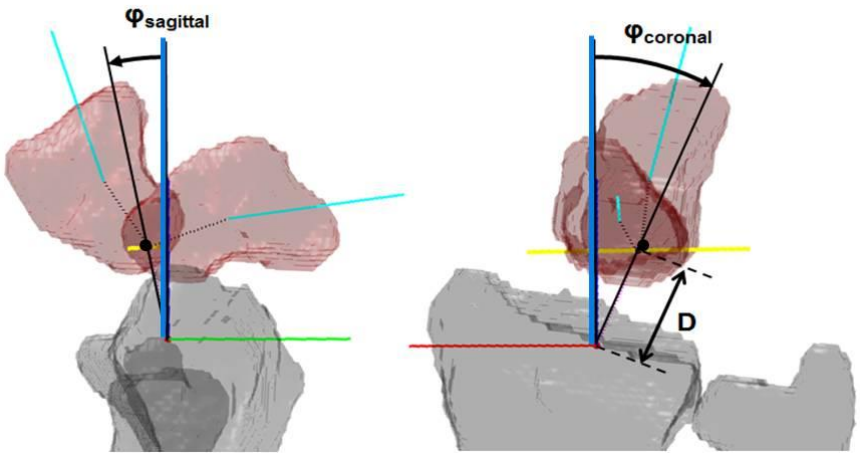

Figure 6. The center of helical axis motion.

The center of helical axis motion (black dot) is presented by the distance (D) from the origin of the reference coordinate system, and the angle from the Z-axis (blue line) in the coronal plane ($\varphi_{coronal}$) and the sagittal plane ($\varphi_{sagittal}$). Red line is X-axis and green line is Y-axis the reference coordinate system.

RESULTS

Radiologically, there was radial inclination averaging 24° (range 20–29°) in the unaffected wrists and 14° (range 8–25°) in the affected wrists. Volar tilt averaged 13° (range 10–17°) in the unaffected wrists, and dorsal tilt averaged 18° (range 10–25°) in the affected wrists. The differences in radial inclination and dorsovolar tilt of the distal radius between the injured and uninjured wrists were statistically significant ($p = 0.0024$ and 0.0000, respectively). Clinically, the average passive range of motion of the injured wrists was 62° extension (range 50–80°), 33° flexion (range 20–50°), 80° supination (range 60–90°), and 83° pronation (range 70–90°), compared to 80° extension (range 70–90°), 80° flexion, 90° supination, and 88° pronation (range 80–90°) of the uninjured wrists.

We calculated the volumes of 8 carpal bones at 5 positions in the same wrist and a representative result is shown in Table 1. The maximum % error of the volumes ranged 0.08–2.44%, and the average and standard deviation of the maximum % error were 1.01% and 0.00496%, respectively.

Table 1. An example of maximum % errors of the estimated volume of the carpal bones.

	Position	Lunate	Scaphoi	Triquetr	Capitat	Hamat	Trap-d	Trap-m	Pisiform
	1	1968.06	2702.88	1626.12	3726.19	3028.06	1191.11	2265.61	1022.41
	2	1962.39	2715.78	1625.21	3720.53	3054.32	1200.62	2268.32	1028.3
	3	1960.58	2702.20	1622.04	3722.12	3063.16	1193.15	2270.59	1026.94
	4	1977.34	2728.01	1626.80	3725.51	3092.14	1214.44	2296.40	1035.09
	5	1957.64	2711.71	1641.52	3720.99	3101.42	1201.53	2276.70	1028.30
	Average	1965.20	2712.12	1628.34	3723.07	3067.82	1200.17	2275.53	1028.21
Rt	SD	6.96	9.49	6.79	2.34	26.48	8.21	11.06	4.06
	Max (+) Error	12.14	15.90	13.18	3.12	33.60	14.27	20.88	6.88
	Max (–) Error	7.56	9.92	6.30	2.54	39.76	9.06	9.92	5.80
	Max % Error	**0.62%**	**0.59%**	**0.81%**	**0.08%**	**1.30%**	**1.19%**	**0.92%**	**0.67%**

The volumes of each carpal bone were calculated in the same wrist of patient 1. Maximum % error was evaluated from the calculated

average, standard deviation and the maximum error.

The projected point on the radial articular surface from the Z-axis was located volar to the origin of the reference coordinate system, and was more volar in the malunited wrist than in the uninjured wrist (Fig. 7).

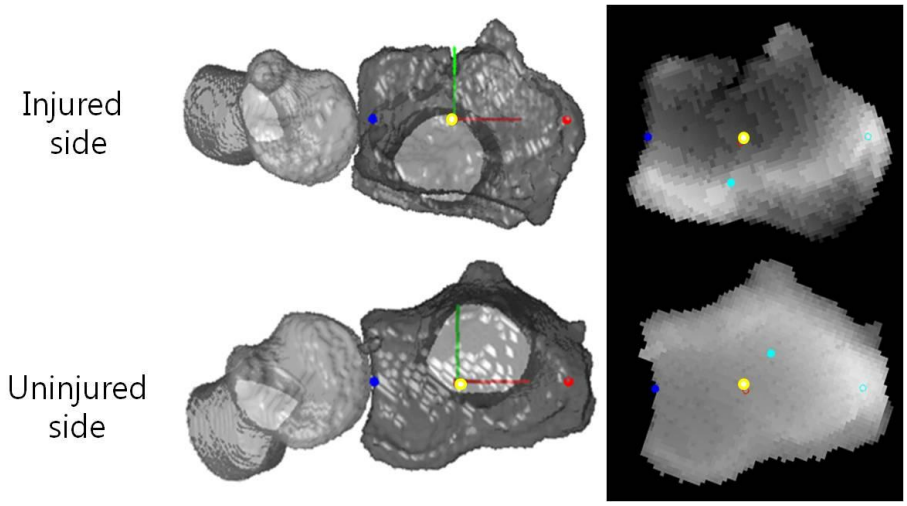

Figure 7. The location of the origin of the coordinate system relative to the Z-axis.

The projected point (skyblue dot) on the radial articular surface from the Z-axis (radial shaft) was located volar to the origin of the coordinate system (yellow dot) and more volarly in the injured than in the uninjured wrist.

The average rotation of the capitate around its own helical axis was 88.87° in the uninjured wrist and 69.96° in the injured wrist, which were significantly different ($p = .0075$). The average translation and lengths of the moment arms were not statistically different between the injured and uninjured wrists. The average rotation, translation, and lengths of the moment arms of the scaphoid and lunate were not significantly different between the injured and uninjured wrists (Table 2).

The capitate was seen to rotate more in the uninjured wrist than in the scaphoid- or lunate-based coordinate system in the uninjured wrist, implying that rotation of the capitate relative to the scaphoid or lunate is smaller in the malunited wrist (Table 3). The length of the moment arm of the capitate in the scaphoid-based coordinate system was larger in the injured wrist.

Table 2. The average rotation, translation, and length of moment arm of the capitate, scaphoid, and lunate around the helical axis in the reference coordinate system. (*p<0.05)

		Rotation (°)		Translation (mm)		Moment arm length (mm)	
		Injured	Uninjured	Injured	Uninjured	Injured	Uninjured
Capitate	Average	69.96	88.87	0.72	0.72	9.08	8.04
	S.D.	15.38	22.98	1.71	1.43	2.92	2.05
	p-value	0.0075*		0.9960		0.1933	
Scaphoid	Average	46.48	54.02	0.35	-0.08	5.28	5.33
	S.D.	16.10	25.05	1.14	1.35	2.16	2.43
	p-value	0.2651		0.1354		0.9363	
Lunate	Average	34.73	33.19	0.96	0.17	3.96	6.09
	S.D.	10.31	13.70	0.95	0.81	1.23	3.23
	p-value	0.6635		0.0956		0.1205	

Table 3. The average rotation, translation, and length of moment arm of the capitate around the helical axis in the scaphoid- and lunate-based coordinate system. (*p<0.05)

		Rotation (°)		Translation (mm)		Moment arm length (mm)	
		Injured	Uninjured	Injured	Uninjured	Injured	Uninjured
Scaphoid-based	Average	26.32	37.77	-0.11	0.08	7.00	6.42
	S.D.	6.77	6.39	0.37	0.33	2.43	1.22
	p-value	0.0289*		0.2337		0.6291	
Lunate-based	Average	39.15	59.34	0.64	0.76	6.27	5.65
	S.D.	4.42	13.6	0.66	0.62	0.36	0.80
	p-value	0.0278*		0.7181		0.0334*	

To summarize rotation of the carpal bones around the helical axis during DTM, radiocapitate, scaphocapitate, and lunocapitate rotation decreased significantly in the injured wrist (Fig. 8–10), while radiolunate and radioscaphoid rotation were not significantly different (Table 4).

Table 4. Radiocarpal and midcarpal rotation during dart-throwing motion. (*p<0.05)

Rotation (°)	R-C (p = 0.0075)*		R-S (p =0.2651)		R-L (p = 0.6635)		S-C (p = 0.0289)*		L-C (p = 0.0278)*	
	Inj	Uninj	Inj	Uninj	Inj	Uninj	Inj	Uninj	Inj	Uninj
Average	69.96	88.87	46.48	54.02	34.73	33.19	26.32	37.77	39.15	59.34
S.D.	15.38	22.98	16.10	25.05	10.31	13.70	6.77	6.39	4.42	13.60

(R-C: radiocapitate; R-S: radioscaphoid; R-L: radiolunate; S-C: scaphocapitate; L-C: lunocapitate)

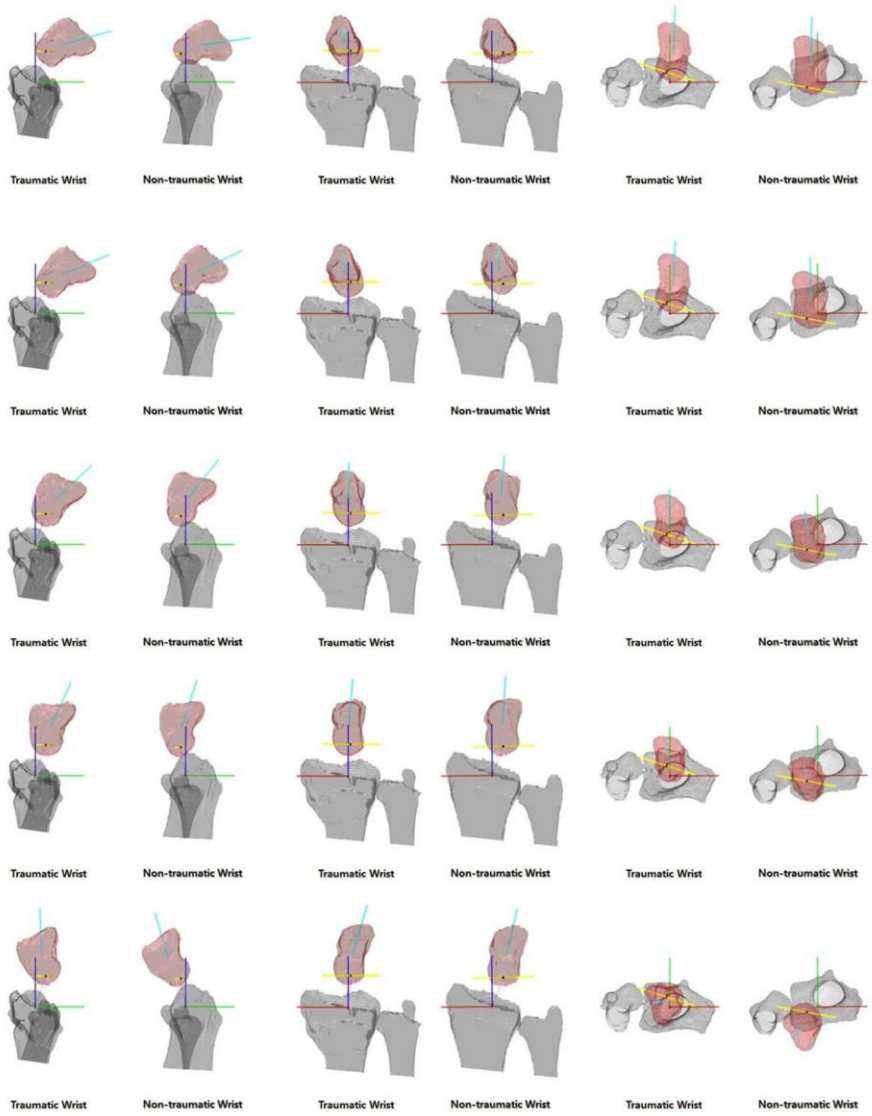

Figure 8. Lateral, volar, and proximal view of rotation of the capitate during dart-throwing motion.

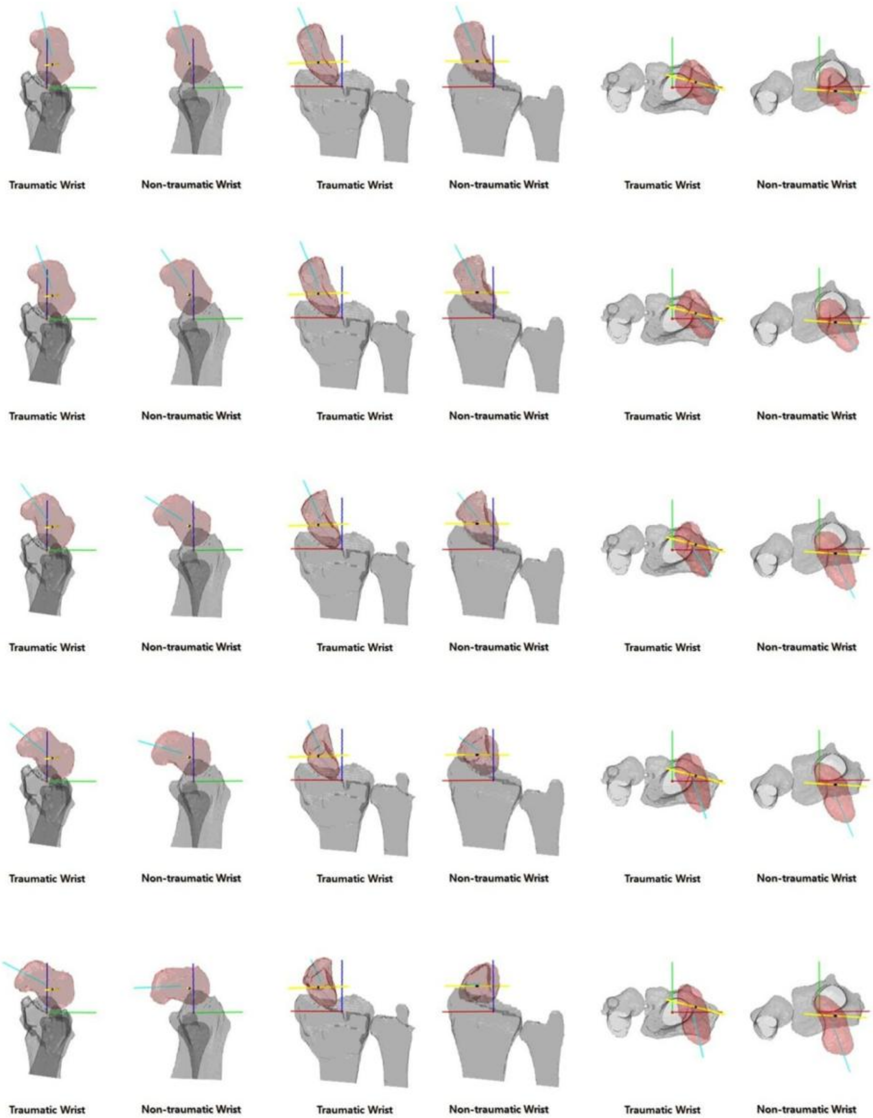

Figure 9. Lateral, volar, and proximal view of rotation of the scaphoid during dart-throwing motion.

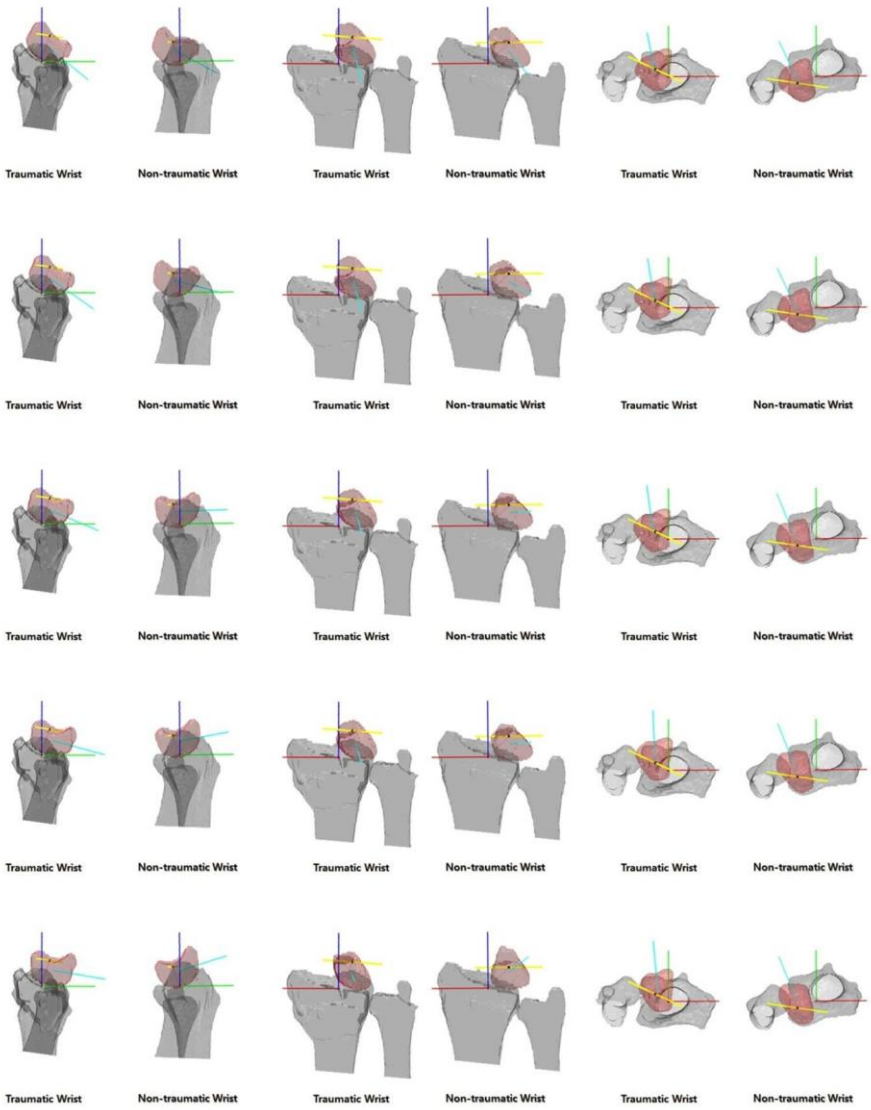

Figure 10. Lateral, volar, and proximal view of rotation of the lunate during dart-throwing motion.

The orientations of the helical axes of the capitate, scaphoid, and lunate by the axial (θ_{XY}), sagittal (θ_{YZ}), and coronal (θ_{ZX}) projection angles did not differ significantly between the injured and uninjured wrists in the reference coordinate system (Table 5). However, the coronal projections between the injured and uninjured wrists were different in the scaphoid- and lunate-based coordinate system (Table 6).

The centers of helical axis motion of the capitate, scaphoid, and lunate were located more dorsally and radially in injured wrists than in uninjured wrists (Fig. 11–13), as the locations were statistically different using the angles from the Z-axis in the coronal ($\varphi_{coronal}$) and sagittal plane ($\varphi_{sagittal}$). The distance from the origin of the coordinate system was not significantly different (Table 7).

Table 5. The orientation of the helical axis of the capitate, scaphoid, and lunate.

		θ_{XY} (°)		θ_{YZ} (°)		θ_{ZX} (°)	
		Inj	Uninj	Inj	Uninj	Inj	Uninj
Capitate	Average	-31.12	-26.82	8.79	-6.23	-34.85	55.85
	S.D.	25.89	17.53	14.97	6.73	78.04	71.26
	p-value	0.4040		0.1038		0.1800	
Scaphoid	Average	-6.54	1.86	11.59	8.27	-82.61	3.68
	S.D.	26.14	36.14	14.69	28.29	5.32	93.49
	p-value	0.1364		0.7593		0.0818	
Lunate	Average	-15.82	-16.80	-1.97	-5.05	2.63	-18.45
	S.D.	24.66	47.76	16.31	13.96	93.21	81.46
	p-value	0.9283		0.7540		0.7040	

The orientation of the helical axis of the three carpal bones was described by the axial (θ_{XY}), sagittal (θ_{YZ}), and coronal projection angle (θ_{ZX}).

Table 6. The orientation of the helical axis of the capitate in the scaphoid- or lunate-based coordinate system. (*p<0.05)

		θ_{XY} (°)		θ_{YZ} (°)		θ_{ZX} (°)	
		Inj	Uninj	Inj	Uninj	Inj	Uninj
Scaphoid-based	Average	-27.07	-31.51	-66.55	-54.79	37.17	48.97
	S.D.	11.35	12.60	16.34	15.19	10.40	6.25
	p-value	0.1331		0.0116*		0.0287*	
Lunate-based	Average	-45.00	-34.59	-50.13	-51.50	40.27	50.01
	S.D.	18.25	13.46	11.60	12.61	10.11	4.99
	p-value	0.0650		0.6876		0.0120*	

The orientation of the helical axis of the three carpal bones in the scaphoid- or lunate-based coordinate system was compared by the axial projection angle (θ_{XY}), the sagittal projection angle (θ_{YZ}), and the coronal projection angle (θ_{ZX}).

Table 7. The center of helical axis motion of the capitate, scaphoid, and lunate. (*p<0.05)

		$\varphi_{coronal}$ (°)		$\varphi_{sagittal}$ (°)		D (mm)	
		Inj	Uninj	Inj	Uninj	Inj	Uninj
Capitate	Average	-0.6	-17.0	17.7	0.3	15.2	15.8
	S.D.	3.7	3.7	9.6	9.5	2.7	2.2
	p-value	0.0004*		0.0033*		0.4948	
Scaphoid	Average	43.6	28.2	4.2	-11.1	14.5	14.4
	S.D.	13.9	15.7	13.4	10.3	1.6	1.7
	p-value	0.0012*		0.0054*		0.9291	
Lunate	Average	-19.7	-31.5	8.8	-18.2	12.4	14.3
	S.D.	6.5	9.4	6.9	5.3	1.4	3.1
	p-value	0.0202*		0.0006*		0.1654	

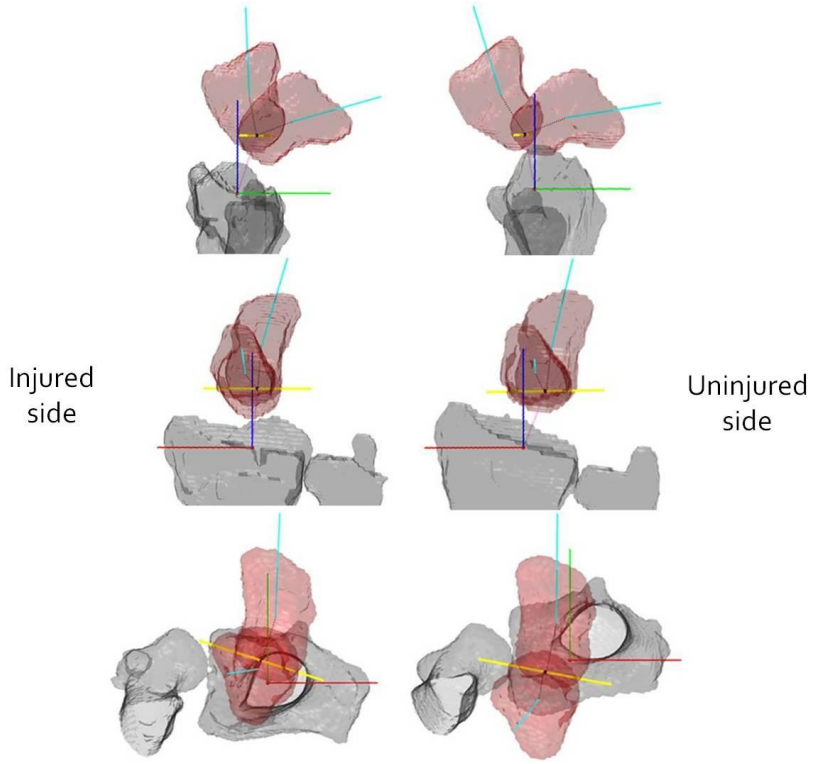

Figure 11. The center of helical axis motion of the capitate.

The center of helical axis motion of the capitate was located more dorsally and radially in injured wrists than in uninjured wrist.

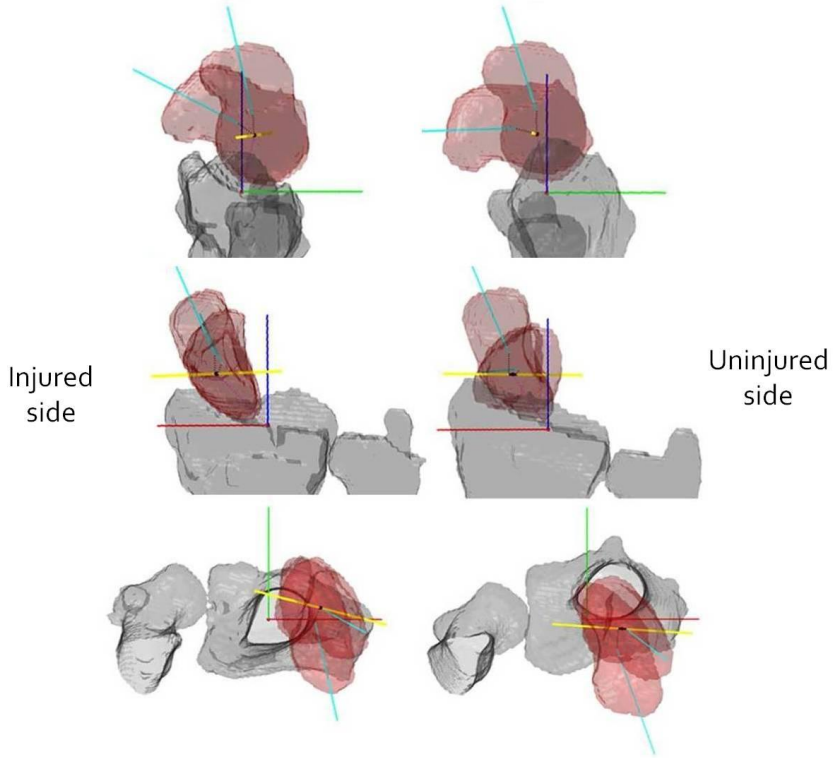

Figure 12. The center of helical axis motion of the scaphoid.

The center of helical axis motion of the scaphoid was located more dorsally and radially in injured wrists than in uninjured wrist.

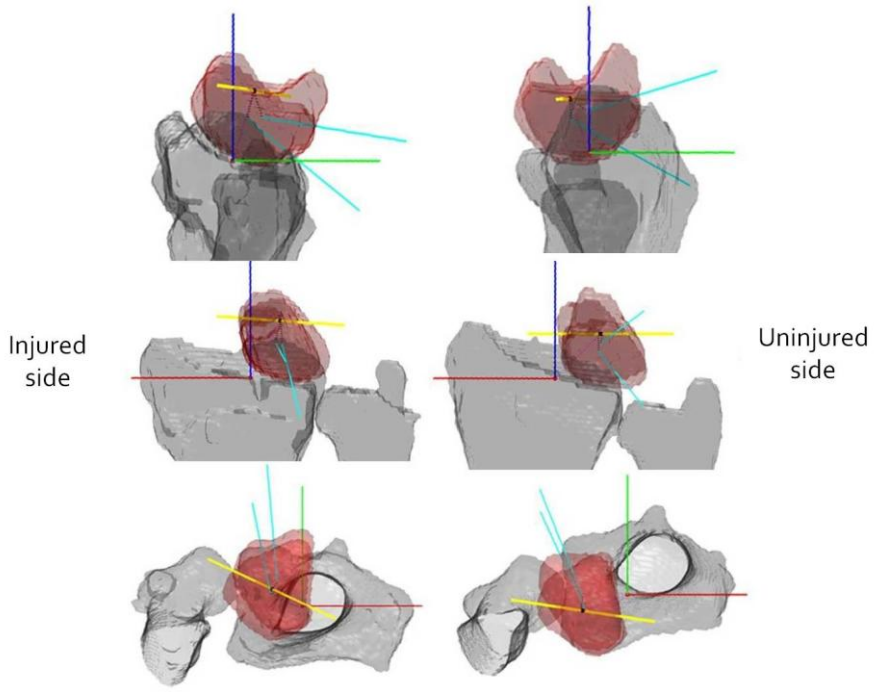

Figure 13. The center of helical axis motion of the lunate.

The center of helical axis motion of the lunate was located more dorsally and radially in injured wrists than in uninjured wrist.

When the radial inclination of the distal radius decreased, $\varphi_{coronal}$ of the capitate, scaphoid, and lunate tended to increase (Fig. 14). When dorsal tilt increased, $\varphi_{sagittal}$ of the capitate, scaphoid, and lunate tended to increase (Fig. 15).

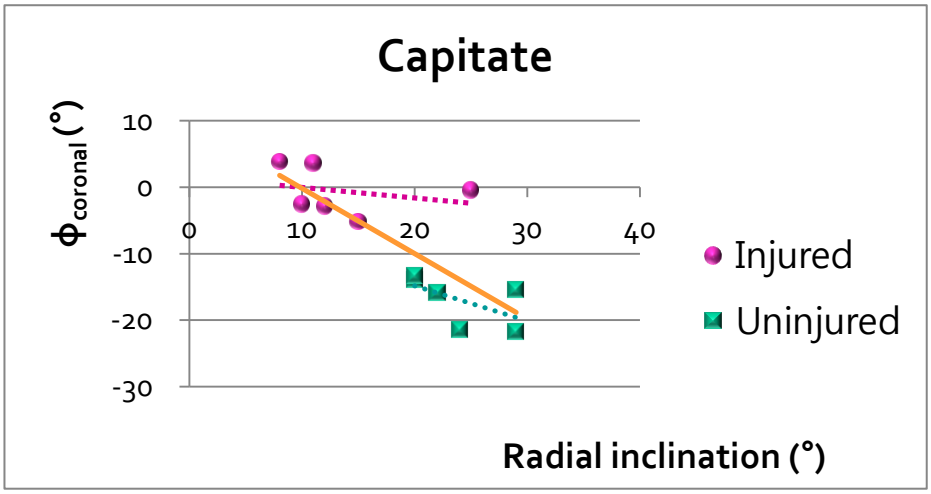
Capitate
ϕcoronal (°)
10
0
-10
-20
-30
0
10
20
30
40
Injured
Uninjured
Radial inclination (°)

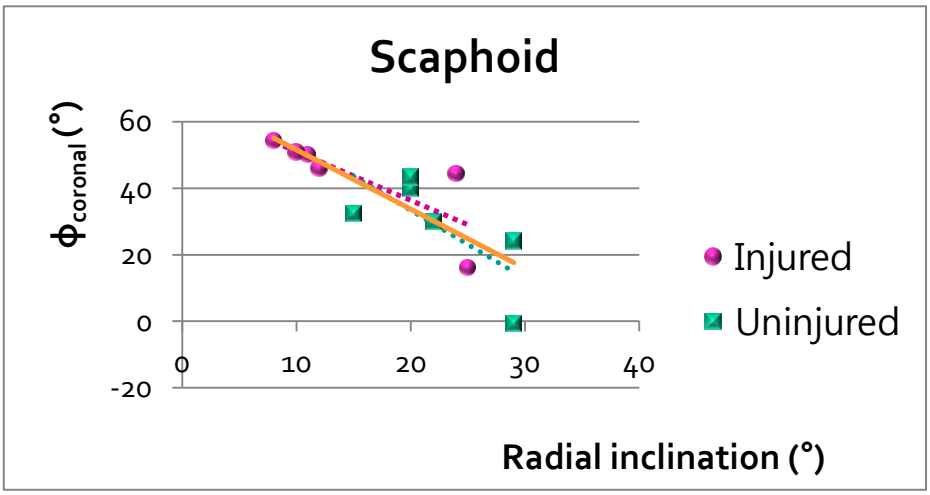
Scaphoid
ϕcoronal (°)
60
40
20
0
-20
0
10
20
30
40
Injured
Uninjured
Radial inclination (°)

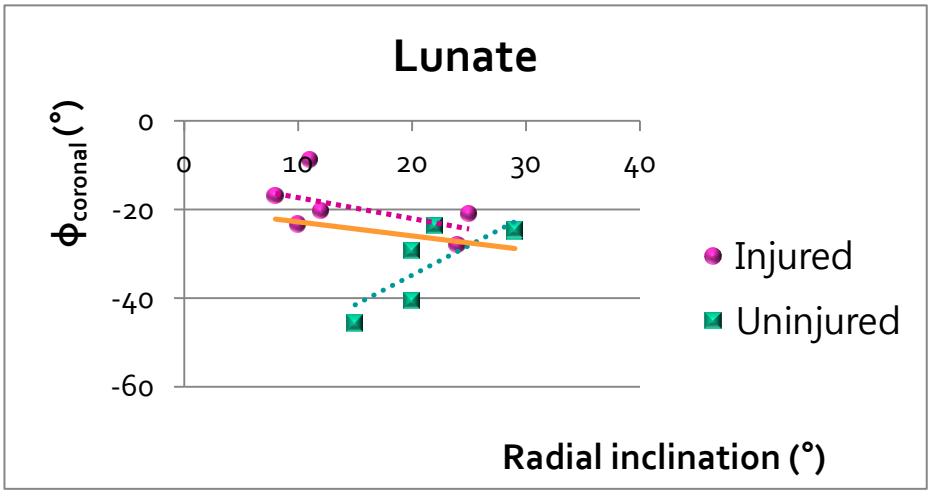
Lunate
ϕcoronal (°)
0
-20
-40
-60
0
10
20
30
40
Injured
Uninjured
Radial inclination (°)

Figure 14. Correlation between radial inclination and $\varphi_{coronal}$ of the capitate, scaphoid, and lunate.

Correlation between radial inclination and $\varphi_{coronal}$ of the capitate, scaphoid, and lunate (Pink dotted line= lineal regression line from data of the injured wrists, green dotted line= line from the uninjured, orange solid line= line from data of the both wrist).

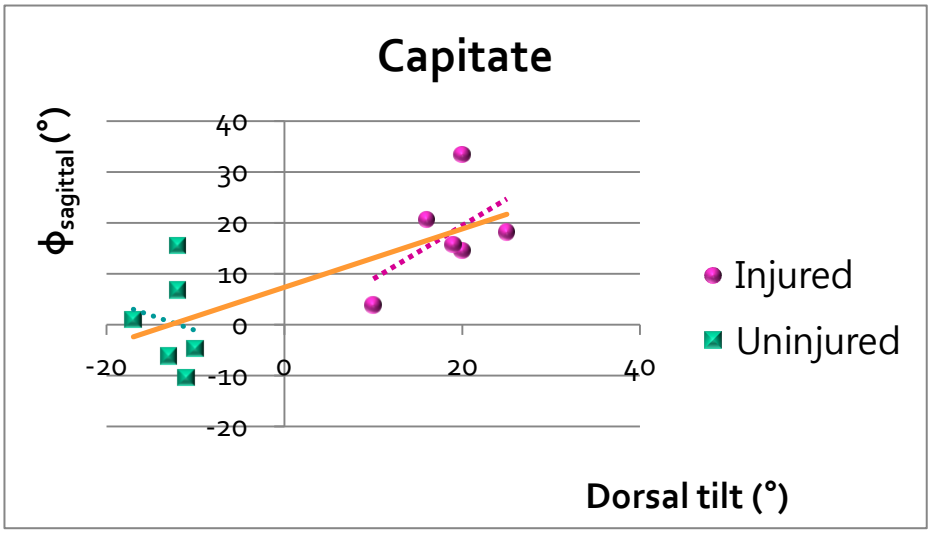

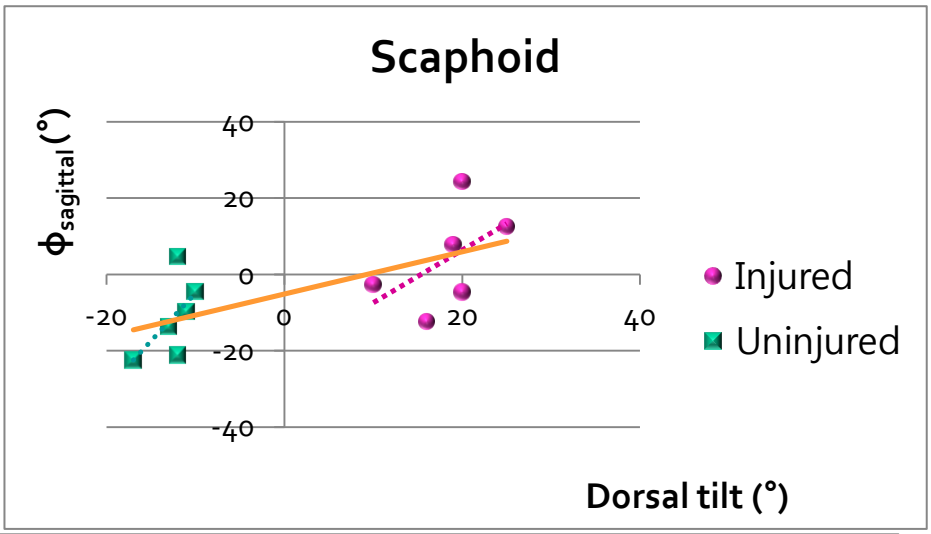

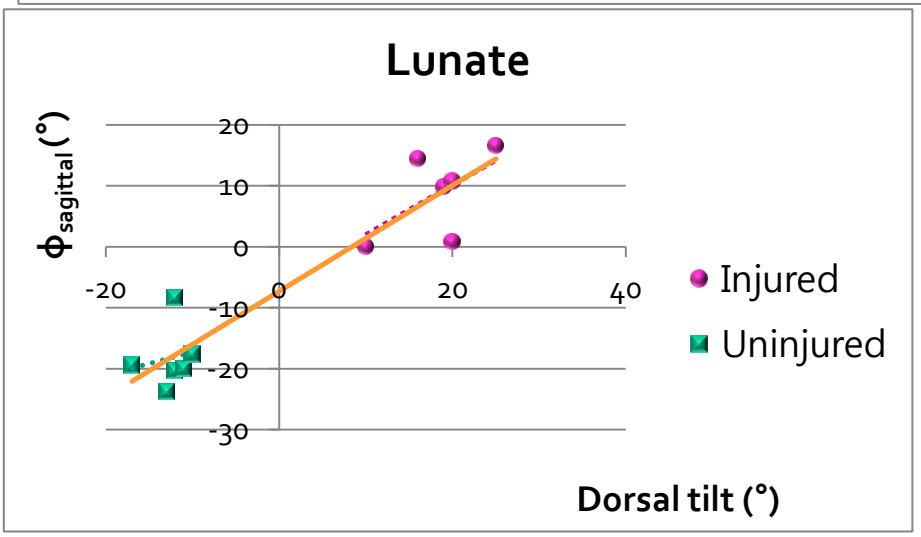

Figure 15. Correlation between dorsal tilt and $\varphi_{sagittal}$ of the capitate, scaphoid, and lunate.

Correlation between dorsal tilt and $\varphi_{sagittal}$ of the capitate, scaphoid, and lunate (Pink dotted line= lineal regression line from data of the injured wrists, green dotted line= line from the uninjured, orange line= line from data of the both wrist).

DISCUSSION

This study presented 3D in vivo kinematics of the capitate, scaphoid, and lunate using noninvasive bone registration techniques from CT images and compared the kinematic parameters between wrists with a distal radius malunion and the contralateral uninjured wrists.

The average and standard deviation of the maximum % error of the technique in this study was 1.01% and 0.00496%. Snel et al[43] estimated average and maximum deviations of the average volume of 8 carpal bones from surface extraction and geometric rendering of MR images, which amounted 1.3% and 3.5%, respectively. In the study of Neu et al,[44] there was a 0.8%–4.8% standard deviation of volume calculations, with larger deviations in smaller bones. The accuracy of the segmentation and rendering technique in this study seem to be satisfactory compared with the results of these 2 previous studies.

The center of the coordinate reference system on the articular surface of the radius was located more dorsally and radially in the malunited wrists than in the contralateral uninjured wrists. This result is compatible with the finding that the fractured distal radius was displaced dorsally and radially in this

study. Further, the shortened distal radius might cause radial displacement of the carpal bones.

The average rotation of the capitate around the helical axis was larger in the uninjured wrist than in the injured wrist, but rotation of the scaphoid and lunate were not significantly different between the sides. The average translations of the capitate, scaphoid, and lunate around their own helical axes were 0.72 ± 1.51, 0.13 ± 1.21, and 0.56 ± 0.94 mm, respectively. If the translation is neglected, the helical axis motion can be regarded as a pure rotation. Therefore, rotation of the capitate around the helical axis could reflect the global wrist motion, which was larger in the uninjured wrist than in the injured, correlating with the clinical measurements of flexion and extension of the wrist. Rotation of the scaphoid and lunate might not be significantly different due to the limited rotation in the DTM plane.

Smaller rotation of the capitate relative to the scaphoid or lunate was observed in the analysis using the scaphoid- or lunate-based coordinate system. As shown in Table 4, radiocapitate, scaphocapitate, and lunocapitate rotation decreased significantly in the injured wrist during DTM, which implied that the decrease of global wrist motion in the wrist with a distal

radius malunion was due to decreased midcarpal motion. This was an interesting result, which might be contrary to the assumption that malunion of the distal radius would affect radiocarpal motion directly and might affect midcarpal motion indirectly through the role of the scaphoid of linkage between the proximal and distal carpal row. The radioscaphoid and radiolunate rotation was minimal during DTM and might decrease minimally, which was not statistically significant. However, this study has shown the importance of midcarpal motion in the decrease of DTM of the wrist with distal radius malunion.

Although the displaced distal radius led to greater dorsal and radial displacement of the center of helical axis motion of the capitate, scaphoid, and lunate, the orientation of the helical axes of the capitate, scaphoid, and lunate were not significantly different. When radial inclination of the distal radius decreased, radial displacement of the center of helical axis motion of the capitate, scaphoid, and lunate tended to increase. When dorsal tilt increased, dorsal displacement of the capitate, scaphoid, and lunate tended to increase. These findings implied that the location of the center of helical axis motion for the carpal bones was related to the severity of the distal radius

malunion.

There have been only 2 studies of 3D CT analysis of distal radius fractures published in English.[27,45] Feipel and Rooze[27] used qualitative and quantitative 3D kinematic analysis with CT data and conducted clinical applications in 25 patients with various wrist disorders such as scaphoid fractures (10 wrists), scapholunate instability (7), radius fracture (7), and ulnar complex lesions (3). They split global rotation and translation about the helical axis into rotations and translations about the anatomical axes of the reference frame and presented average and standard deviations of rotation components of the scaphoid, triquetrum, and hamate in symptomatic wrists with scaphoid lesions. Because they performed quantitative kinematic study only with scaphoid lesions, there was no carpal kinematic analysis of distal radius fracture reported in their study.

Crisco et al[45] studied the effects of distal radius malunion on distal radioulnar joint mechanics and reported that the ulnar joint space area was significantly decreased, the centroid of this area moved an average of 1.3 mm proximally, and the dorsal radioulnar ligament elongated. The 3D kinematic analysis was performed in the distal radioulnar joint, and no

kinematic data of carpal bones were provided. Thus, the present study might be the first 3D kinematic analysis of the effect of distal radius malunion on the carpal bones.

There are limitations in this study. First, the patients in this study had radiologically significant malunions of the distal radius, but did not have severe functional disabilities. More severe malunions might be associated with more pronounced functional limitations and greater limitation of wrist motion. Second, there may be individual variations of biomechanical factors affecting carpal bone motions, such as ligament laxity, and there might be differences between the right and left wrists, even in the same patients, depending on handedness. Third, there might be differences between dynamically and statically acquired carpal kinematics. DTM is dynamic, continuous motion in reality, but CT scanning was performed in 5 step-wise positions, which could not provide real carpal motions. Foumani et al[46] observed small, and in most cases negligible, differences between the dynamic motion and the step-wise static motion of the carpal bones in the evaluation of individuals without any pathology of the wrist. They suggested that further research would be required to investigate dynamic in vivo carpal

kinematics in patients with dynamic wrist problems.

Fourth, the helical axis motions were analyzed from only 2 extreme positions (positions 1 and 5) in this study. This could not reflect the gradual changes of the carpal bone motion during DTM. Fifth, as the study included only 6 patients and 12 wrists, the statistical analysis had limited power. The patients had distal radius malunions of varying severity, and the main displacement was dorsal in some cases and radial in others. When more patients are analyzed, it may provide further evidence that the severity and direction of distal radius malunion is associated with changes in carpal kinematics. Sixth, the status of intrinsic and extrinsic ligaments was not evaluated in this study. The carpal ligaments might have been injured when the distal radius was fractured and this could have an influence on the carpal bone motion. Evaluation of carpal bone instability on physical examination and radiography were used to exclude ligament instability in the wrists, but some wrists may still have had low grade ligament injury

This 3D in vivo kinematic study of the capitate, scaphoid, and lunate in wrists with distal radius malunion might be the first to present a 3D kinematic analysis of the effect of distal radius malunion on the carpal bones.

This study showed that decreased DTM in wrists with a distal radius malunion resulted from decreased midcarpal motion. The capitate is a key carpal bone in midcarpal motion and DTM. Therefore, capitate motion should be observed carefully to evaluate the functional motion of any injured wrist. The motion analysis in wrist kinematics studies should be performed in the DTM plane as well as in conventional flexion-extension and radial-ulnar deviation, which are not the functional directions in virtual wrist motion.

DTM is a crucial motion of the wrist joint in activities of daily living and occupational tasks, and the present result indicates that anatomical reduction of distal radius fractures should be performed to maintain the function of the wrist. DTM and capitate motion should be parameters to evaluate the function of a wrist with a distal radius fracture or malunion.

REFERENCES

1. Forward DP, Davis TR, Sithole JS. 2008. Do young patients with malunited fractures of the distal radius inevitably develop symptomatic post-traumatic osteoarthritis? J Bone Joint Surg Br 90: 629-637.

2. Foldhazy Z, Tornkvist H, Elmstedt E, et al. 2007. Long-term outcome of nonsurgically treated distal radius fractures. J Hand Surg Am 32: 1374-1384.

3. Bickerstaff DR, Bell MJ. 1989. Carpal malalignment in Colles' fractures. J Hand Surg Br 14: 155-160.

4. Jenkins NH, Mintowt-Czyz WJ. 1988. Mal-union and dysfunction in Colles' fracture. J Hand Surg Br 13: 291-293.

5. McQueen M, Caspers J. 1988. Colles fracture: does the anatomical result affect the final function? J Bone Joint Surg Br 70: 649-651.

6. Solgaard S. 1988. Function after distal radius fracture. Acta Orthop Scand 59: 39-42.

7. Verhaegen F, Degreef I, De Smet L. 2010. Evaluation of corrective osteotomy of the malunited distal radius on midcarpal and radiocarpal malalignment. J Hand Surg Am 35: 57-61.

8. Taleisnik J, Watson HK. 1984. Midcarpal instability caused by malunited

fractures of the distal radius. J Hand Surg Am 9: 350-357.

9. Amadio PC, Botte MJ. 1987. Treatment of malunion of the distal radius. Hand Clin 3: 541-561.

10. Linscheid RL, Dobyns JH, Beabout JW, Bryan RS. 1972. Traumatic instability of the wrist. Diagnosis, classification, and pathomechanics. J Bone Joint Surg Am 54: 1612-1632.

11. Fernandez DL. 1993. Malunion of the distal radius: current approach to management. Instr Course Lect 42: 99-113.

12. Park MJ, Cooney WP, 3rd, Hahn ME, et al. 2002. The effects of dorsally angulated distal radius fractures on carpal kinematics. J Hand Surg Am 27: 223-232.

13. Jupiter JB, Fernandez DL. 2002. Complications following distal radial fractures. Instr Course Lect 51: 203-219.

14. af Ekenstam F, Hagert CG, Engkvist O, et al. 1985. Corrective osteotomy of malunited fractures of the distal end of the radius. Scand J Plast Reconstr Surg 19: 175-187.

15. Melendez EM. 1997. Opening-wedge osteotomy, bone graft, and external fixation for correction of radius malunion. J Hand Surg Am 22: 785-

791.

16. Posner MA, Ambrose L. 1991. Malunited Colles' fractures: correction with a biplanar closing wedge osteotomy. J Hand Surg Am 16: 1017-1026.

17. Watson HK, Castle TH, Jr. 1988. Trapezoidal osteotomy of the distal radius for unacceptable articular angulation after Colles' fracture. J Hand Surg Am 13: 837-843.

18. Fernandez DL. 1982. Correction of post-traumatic wrist deformity in adults by osteotomy, bone-grafting, and internal fixation. J Bone Joint Surg Am 64: 1164-1178.

19. Short WH, Palmer AK, Werner FW, Murphy DJ. 1987. A biomechanical study of distal radial fractures. J Hand Surg Am 12: 529-534.

20. Palmer AK, Werner FW, Murphy D, Glisson R. 1985. Functional wrist motion: a biomechanical study. J Hand Surg Am 10: 39-46.

21. Crisco JJ, Wolfe SW, Neu CP, Pike S. 2001. Advances in the in vivo measurement of normal and abnormal carpal kinematics. Orthop Clin North Am 32: 219-231, vii.

22. Goto A, Moritomo H, Murase T, et al. 2005. In vivo three-dimensional wrist motion analysis using magnetic resonance imaging and volume-based

registration. J Orthop Res 23: 750-756.

23. Wolfe SW, Crisco JJ, Orr CM, Marzke MW. 2006. The dart-throwing motion of the wrist: is it unique to humans? J Hand Surg Am 31: 1429-1437.

24. Capener N. 1956. The hand in surgery. J Bone Joint Surg Br 38-B: 128-151.

25. Wolfe SW, Crisco JJ, Katz LD. 1997. A non-invasive method for studying in vivo carpal kinematics. J Hand Surg Br 22: 147-152.

26. Crisco JJ, McGovern RD, Wolfe SW. 1999. Noninvasive technique for measuring in vivo three-dimensional carpal bone kinematics. J Orthop Res 17: 96-100.

27. Feipel V, Rooze M. 1999. Three-dimensional motion patterns of the carpal bones: an in vivo study using three-dimensional computed tomography and clinical applications. Surg Radiol Anat 21: 125-131.

28. Snel JG, Venema HW, Moojen TM, et al. 2000. Quantitative in vivo analysis of the kinematics of carpal bones from three-dimensional CT images using a deformable surface model and a three-dimensional matching technique. Medical physics 27: 2037-2047.

29. Wolfe SW, Neu C, Crisco JJ. 2000. In vivo scaphoid, lunate, and capitate

kinematics in flexion and in extension. J Hand Surg Am 25: 860-869.

30. Moritomo H, Goto A, Sato Y, et al. 2003. The triquetrum-hamate joint: an anatomic and in vivo three-dimensional kinematic study. J Hand Surg Am 28: 797-805.

31. Neu CP, Crisco JJ, Wolfe SW. 2001. In vivo kinematic behavior of the radio-capitate joint during wrist flexion-extension and radio-ulnar deviation. J Biomech 34: 1429-1438.

32. Moojen TM, Snel JG, Ritt MJ, et al. 2002. Three-dimensional carpal kinematics in vivo. Clin Biomech (Bristol, Avon) 17: 506-514.

33. Moritomo H, Murase T, Goto A, et al. 2006. In vivo three-dimensional kinematics of the midcarpal joint of the wrist. J Bone Joint Surg Am 88: 611-621.

34. Leventhal EL, Moore DC, Akelman E, et al. 2010. Carpal and forearm kinematics during a simulated hammering task. J Hand Surg Am 35: 1097-1104.

35. Moritomo H, Murase T, Goto A, et al. 2004. Capitate-based kinematics of the midcarpal joint during wrist radioulnar deviation: an in vivo three-dimensional motion analysis. J Hand Surg Am 29: 668-675.

36. Moritomo H, Viegas SF, Elder K, et al. 2000. The scaphotrapezio-trapezoidal joint. Part 2: A kinematic study. J Hand Surg Am 25: 911-920.

37. Li ZM, Kuxhaus L, Fisk JA, Christophel TH. 2005. Coupling between wrist flexion-extension and radial-ulnar deviation. Clin Biomech (Bristol, Avon) 20: 177-183.

38. Werner FW, Short WH, Fortino MD, Palmer AK. 1997. The relative contribution of selected carpal bones to global wrist motion during simulated planar and out-of-plane wrist motion. J Hand Surg Am 22: 708-713.

39. Ishikawa J, Cooney WP, 3rd, Niebur G, et al. 1999. The effects of wrist distraction on carpal kinematics. J Hand Surg Am 24: 113-120.

40. Werner FW, Green JK, Short WH, Masaoka S. 2004. Scaphoid and lunate motion during a wrist dart throw motion. J Hand Surg Am 29: 418-422.

41. Crisco JJ, Coburn JC, Moore DC, et al. 2005. In vivo radiocarpal kinematics and the dart thrower's motion. J Bone Joint Surg Am 87: 2729-2740.

42. Panjabi MM, Krag MH, Goel VK. 1981. A technique for measurement and description of three-dimensional six degree-of-freedom motion of a

body joint with an application to the human spine. J Biomech 14: 447-460.

43. Snel JG, Venema HW, Grimbergen CA. 2002. Deformable triangular surfaces using fast 1-D radial Lagrangian dynamics--segmentation of 3-D MR and CT images of the wrist. IEEE Trans Med Imaging 21: 888-903.

44. Neu CP, McGovern RD, Crisco JJ. 2000. Kinematic accuracy of three surface registration methods in a three-dimensional wrist bone study. J Biomech Eng 122: 528-533.

45. Crisco JJ, Moore DC, Marai GE, et al. 2007. Effects of distal radius malunion on distal radioulnar joint mechanics--an in vivo study. J Orthop Res 25: 547-555.

46. Foumani M, Strackee SD, Jonges R, et al. 2009. In-vivo three-dimensional carpal bone kinematics during flexion-extension and radio-ulnar deviation of the wrist: Dynamic motion versus step-wise static wrist positions. J Biomech 42: 2664-2671.

국문 초록

서론: 이 연구의 목적은 원위 요골 부정유합을 가진 수근 관절과 반대편 정상 수근 관절 간의 다트 던지기 운동에서의 유두골, 주상골 및 월상골의 운동을 전산화 단층 영상을 이용하여 삼차원 동력학적으로 분석으로 비교하는 것이다.

방법: 일측 원위 요골 부정유합을 가진 6명의 환자에서 다트 던지기 운동을 수행하면서 5단계 연속 위치에서 양측 수근 관절에 동시에 전산화 단층 촬영을 시행하였다. 나선 축 운동의 개념을 이용하여 유두골, 주상골 및 월상골의 평균 회전, 전위 및 모멘트 팔의 길이를 계산하고 양측 수근관절의 비교를 시행하였다. 유두골의 나선 운동을 또한 주상골 중심과 월상골 중심의 좌표계에서 평가하였다. 나선 축 운동의 축의 방향과 운동의 중심의 위치를 양측 수근관절에서 비교하였다.

결과: 유두골의 나선 축 주변의 평균 회전은 정상 수근 관절에서 손상 수근 관절보다 컸으나, 평균 전위와 모멘트 팔의 길이는 통계적으로 차이가 없었다. 주상골과 월상골에서는 평균 회전, 전위 및 모멘트 팔의 길이는 양측 수근 관절에서 유의한 차이가 없었다. 주상골 중심 및 월상골 중심의 좌표계에서 유두골은 정상 수근 관절에서 더 많이 회전하였다. 유두골, 주상골, 월상골의 나선 축의 방향은 유의한 차이가 없었다. 손상 수근 관절에서 세 수근골의 나선 축 운동의 중심은 더 배측 및 외측에 위치하였다. 원위 요골의 요측 경사가 감소할수록 세 수근골의 나선 운동의

중심의 요측 전위는 더 증가하는 경향을 보였다. 배측 경사가 증가할수록 세 수근골의 운동 중심의 배측 전위는 더 증가하였다.

결론: 원위 요골 부정유합을 가진 수근 관절에서 다트 던지기 운동의 감소는 중수근 관절 운동의 감소에 의한 것으로 관찰되었다. 따라서, 수근 관절의 기능에 중요한 다트 던지기 운동을 보존하기 위하여 원위 요골의 골절의 해부학적인 정복이 필요하다.

주요어: 원위 요골 부정유합, 다트 던지기 운동, 수근관절 동역학, 삼차원, 전산화 단층 촬영.

학 번: 2007-30509